

H₂ molecular gas absorption-selected systems trace CO molecular gas-rich galaxy overdensities

Anne Klitsch,^{1*} Céline Péroux,^{2,3} Martin A. Zwaan,² Annalisa De Cia,⁴ Cédric Ledoux,⁵ Sebastian Lopez⁶

¹*DARK, Niels Bohr Institute, University of Copenhagen, Jagtvej 128, 2200 Copenhagen, Denmark*

²*European Southern Observatory, Karl-Schwarzschildstrasse 2, D-85748 Garching bei München, Germany*

³*Aix Marseille Univ, CNRS, CNES, LAM, (Laboratoire d'Astrophysique de Marseille), UMR 7326, 13388, Marseille, France*

⁴*Department of Astronomy, University of Geneva, Chemin Pegasi 51, 1290 Versoix, Switzerland*

⁵*European Southern Observatory, Alonso de Córdova 3107, Casilla 19001, Vitacura, Santiago, Chile*

⁶*Departamento de Astronomía, Universidad de Chile, Casilla 36-D, Santiago, Chile*

Accepted 2021 June 5. Received 2021 June 4; in original form 2021 January 20.

ABSTRACT

Absorption-selected galaxies offer an effective way to study low-mass galaxies at high redshift. However, the physical properties of the underlying galaxy population remains uncertain. In particular, the multiphase circum-galactic medium is thought to hold key information on gas flows into and out of galaxies that are vital for galaxy evolution models. Here we present ALMA observations of CO molecular gas in host galaxies of H₂-bearing absorbers. In our sample of six absorbers we detect molecular gas-rich galaxies in five absorber fields although we did not target high-metallicity (> 50 per cent solar) systems for which previous studies reported the highest detection rate. Surprisingly, we find that the majority of the absorbers are associated with multiple galaxies rather than single haloes. Together with the large impact parameters these results suggest that the H₂-bearing gas seen in absorption is not part of an extended disk, but resides in dense gas pockets in the circum-galactic and intra-group medium.

Key words: quasars: absorption lines – galaxies: ISM – galaxies: groups – ISM: molecules

1 INTRODUCTION

Conventional surveys identify galaxies based on the continuum or line emission and are therefore preferentially select the most luminous part of the galaxy populations. These are high stellar mass and star-formation rate galaxies. An alternative galaxy selection technique is based on the absorption signature that the gas content imprints in the spectra of otherwise unrelated background quasars (damped Ly α absorbers with a column density of HI > 2×10^{20} cm⁻² Wolfe et al. 2005). The absorption traces the neutral HI gas in galaxies. Damped Ly α absorbers trace the majority of HI in the Universe, as well as the majority of metals at high redshift (Péroux & Howk 2020). These absorption-selected galaxies include the selection of lower-mass galaxies that lie at or below the main sequence for star-forming galaxies at their respective redshifts (e.g. Kanekar et al. 2018; Rhodin et al. 2018).

Therefore, a good understanding of the underlying galaxy population traced by absorption-selection is required to draw firm conclusions on the evolution of the whole galaxy population. It has been suggested that absorption-selected galaxies at intermediate redshift ($z \sim 0.5$) are extremely molecular gas-rich and have a low star formation efficiency compared to emission-selected galaxies at low ($z \sim 0$) and high ($z \sim 2$) redshift (Kanekar et al. 2018; Kanekar et al. 2020). The authors of these studies selected high metallicity absorbers and

report CO detection rates of 40–70 per cent. In another sample of six absorption-selected galaxies observed with MUSE and ALMA, the MUSE-ALMA Halos survey, Szakacs et al. (2021) report a CO detection rate of 1/3. However, in total only small samples of molecular gas mass measurements at low, intermediate and high redshifts are available.

At the same time the advent of large field-of-view integral field spectrographs in the optical such as the Multi Unit Spectroscopic Explorer (MUSE) on the VLT and the Keck Cosmic Web Imager (KCWI) on the Keck II telescope enabled efficient detection of absorber host galaxies with star-formation rate limits of $\sim 0.1 M_{\odot} \text{yr}^{-1}$. These surveys have revealed an increasing number of absorbers associated to groups of galaxies rather than individual systems (e.g. Bielby et al. 2017; Péroux et al. 2017; Klitsch et al. 2018; Péroux et al. 2019; Hamanowicz et al. 2020; Schroetter et al. 2021; Loft-house et al. 2020). Recently, a group of nine galaxies associated with an H₂ absorber within 600 proper kpc tracing a galaxy overdensity was presented by Boettcher et al. (2020).

A growing sample of molecular gas observations in absorption-selected systems is now available (e.g. Neeleman et al. 2016; Neeleman et al. 2018; Møller et al. 2018; Klitsch et al. 2018, 2019; Kanekar et al. 2018; Kanekar et al. 2020; Fynbo et al. 2018; Szakacs et al. 2021) Only in two absorption-selected systems more than one molecular gas-rich galaxy have been reported in emission (Klitsch et al. 2019; Péroux et al. 2019). However, a systematic study in CO emis-

* E-mail: anne.klitsch@gmail.com

sion observed with ALMA similar to those for ionised gas carried out in the optical with MUSE is still missing.

The goal of this study is to follow-up Ly α absorbers with previously identified H₂ absorption identified from UV absorption lines. The presence of H₂-bearing gas in absorption potentially suggests a large reservoir of molecular gas also observable in CO emission. We search for molecular gas emission from the absorber host galaxy(s) and aim to identify the origin of the absorbing gas.

This paper is organised as follows: In Section 2 we describe the target selection, observations and data reduction, the detected galaxies and the relations between the absorbing gas and the host galaxies are presented in Section 3 and in Section 4 we give a summary of this work and list our conclusions.

Throughout the paper we adopt a Λ CDM cosmological model with $H_0 = 70 \text{ km s}^{-1} \text{ Mpc}^{-1}$, $\Omega_m = 0.3$, and $\Omega_\Lambda = 0.7$.

2 OBSERVATIONS AND DATA REDUCTION

2.1 Target selection

The absorbers were selected to have an H₂ molecular gas absorption detection at UV wavelength. Additionally, we selected absorbers observable with ALMA and at $z \lesssim 1$ to limit the required observing time. The neutral gas column densities of these absorbers are in the range of $\log(N(\text{HI})/\text{cm}^{-2}) = 19.00 - 20.50$ and the molecular fractions cover a range of $\log f_{\text{mol}} = -4$ to -0.4 . We find that although it was not a selection parameter, some absorbers in our sample have a high metallicity of above 30 per cent solar, but we also include low metallicity systems with only ~ 10 per cent of solar metallicity. We note that some of these metallicity estimates do not include ionisation corrections and could therefore be somewhat higher. This distribution is expected for a sample of H₂ absorbers (Bolmer et al. 2019). The absorber properties including optically identified host galaxies are listed in Table 1.

2.2 ALMA observations

The six target fields are listed in Table 1. We observe the lowest possible CO transition for each absorber where the specific transition is determined by the absorber redshift (z_{abs}). The lowest CO transition is observed to minimize uncertainties from the line luminosity conversion, needed to evaluate the total molecular gas mass. The observations are carried out under program 2018.1.01575.S (PI Klitsch). All observations use four ALMA 1.875 GHz bands, with one band (in spectral-line mode of the correlator) covering the respective expected redshifted CO line frequency, and the other three bands (in continuum mode) placed at neighbouring frequencies to measure the continuum emission. We start the data reduction with the pipeline calibrated uv-data sets, as delivered by ALMA. Additional data reduction steps are carried out with the Common Astronomy Software Applications (CASA) software package version 5.6 (McMullin et al. 2007). The imaging is done using the standard *tclean* algorithm with a final field of view of 1.5 times the primary beam size. This results in an image diameter of 1.4' in ALMA Band 3 and 1.2' in ALMA Band 4. A 'natural' weighting scheme is applied, which guarantees optimal sensitivity appropriate for a line detection experiment. The final beam sizes as well as the rms noise are listed in Table 2. We use a channel width of 15 - 20 km s^{-1} .

2.3 Archival MUSE observations

One of the ALMA targets (HE 0515-4414) was observed with MUSE under the project ID: 1100.A-0528 (PI: Fumagalli). The MUSE FoV covers a $1' \times 1'$ area, slightly narrower than that of our ALMA observations. We have downloaded the pipeline-processed and flux calibrated data cube from the ESO Phase 3 archive. We use this data to search for optical counterparts for the CO detected galaxies.

3 RESULTS

We search for CO line emission in the ALMA image cubes before correcting for the primary beam response to ensure constant noise properties across the field of view. We search for line emission both by-eye and using the line finder software SoFIA and detect CO line emission in four out of six absorber fields. We find in total nine galaxies. Three out of four absorbers have more than one galaxy in close proximity. In addition to the detections from this work we use the results for Q2131-1207 presented by Szakacs et al. (2021). The properties of our detections are listed in table 3.

The velocity profiles of the detected galaxies have a FWHM of 60–500 km s^{-1} . Previously reported CO detections of absorption selected galaxies have a FWHM of $> 300 \text{ km s}^{-1}$ (e.g. Kanekar et al. 2018; Kanekar et al. 2020; Klitsch et al. 2018, 2019; Møller et al. 2018; Péroux et al. 2019). While the narrow CO emission lines could trace low mass galaxies we also note that the detection is only significant over few channels in the ALMA data. Therefore, we flag galaxies with a FWHM $< 300 \text{ km s}^{-1}$ as low significance detections unless the detection is confirmed by independent observations. These are still included in the further analysis to avoid a bias against low mass galaxies. When studying trends and drawing general conclusions we regard both, the high significance sample only and the full sample.

3.1 Notes on the individual quasar fields

Emission line maps and extracted spectra of the detections are shown in Fig. 1 and 2. The relation between the CO detection and the absorber in velocity space is illustrated in Fig. 3. The CO spectra are obtained from the primary beam corrected image cubes. Since many sources are resolved we integrate the spectra over a region defined by the 3σ contour in the integrated flux map. We do not detect significant continuum emission from any galaxy detected in CO. A detailed analysis of the different fields is presented in the following.

B0120-28 ($z_{\text{abs}} = 0.18562$) We do not detect a host galaxy associated with the absorber in this field. Oliveira et al. (2014) report an absorber host galaxy at an impact parameter of 70 kpc based on imaging and spectroscopic data. However, the full details of this galaxy remain unpublished. We have therefore calculated an upper limit on the molecular gas mass based on the sensitivity limit of our CO(1–0) emission line observations.

J1342-0053 ($z_{\text{abs}} = 0.22711$) We report a detection of CO(1–0) emission coincident with a previously optically identified absorber host galaxy (Werk et al. 2013). The authors report a SFR of $6.04 M_\odot \text{ yr}^{-1}$, a stellar mass of $10^{10.93} M_\odot$, a luminosity of $1.08 L^*$, and a super solar metallicity of $12 + \log(\text{O}/\text{H}) = 9.05$.

Q2131-1207 ($z_{\text{abs}} = 0.4298$) We do not detect CO(2–1) emission in the field of Q2131-1207 at the sensitivity limit of our observations. This field has been observed with VLT/MUSE presented by Péroux

Table 1. Physical properties of quasar absorbers targeted in this sample.

Field	Alternative Name	z_{QSO}	z_{abs}	$\log(N(\text{HI})/\text{cm}^{-2})$	$\log(N(\text{H}_2)/\text{cm}^{-2})$	$\log Z/Z_{\odot}$	Θ [kpc]
QSO B0120-28		0.434	0.18561	20.50 ± 0.10^d	20.00 ± 0.10^d	-1.19 ± 0.21^d	70^d
J1342-0053	LBQS 1340-0038	0.326	0.22711	$19.0^{+0.5}_{-0.8}^e$	14.63 ± 0.06^a	$-0.40^{+0.40}_{-0.10}^k$	35^e
Q2131-1207	PKS 2128-123	0.500	0.4298	19.5 ± 0.15^j	16.36 ± 0.08^j	$> -0.96^b$	$12, 48^f$
Q1241+176	QSO J1244+1721	1.273	0.55048	$> 19.00^i$	15.81 ± 0.17^a	$< 0.18^a$	21^g
Q0107-0232	LBQS 0107-0232	0.728	0.55733	19.50 ± 0.20^h	17.27 ± 0.30^h	-0.72 ± 0.32^h	$10, 11^h$
HE 0515-4414	QSO B0515-4414	1.713	1.15	19.88 ± 0.05^c	$16.94^{+0.23}_{-0.41}^c$	-0.38 ± 0.04^l	

Notes: Θ denotes the impact parameter between the quasar sight-line and a previously identified absorber host galaxy. **References:** ^a Average metallicities ([S/H] or [Si/H]) from Muzahid et al. (2015) without ionization correction, ^b Som et al. (2015), ^c Reimers et al. (2003), ^d Oliveira et al. (2014), ^e Werk et al. (2013), ^f Péroux et al. (2017), ^g Steidel et al. (1994), ^h Crighton et al. (2013), ⁱ Rao et al. (2006), ^j Muzahid et al. (2016), ^k Werk et al. (2014), ^l Quast et al. (2008)

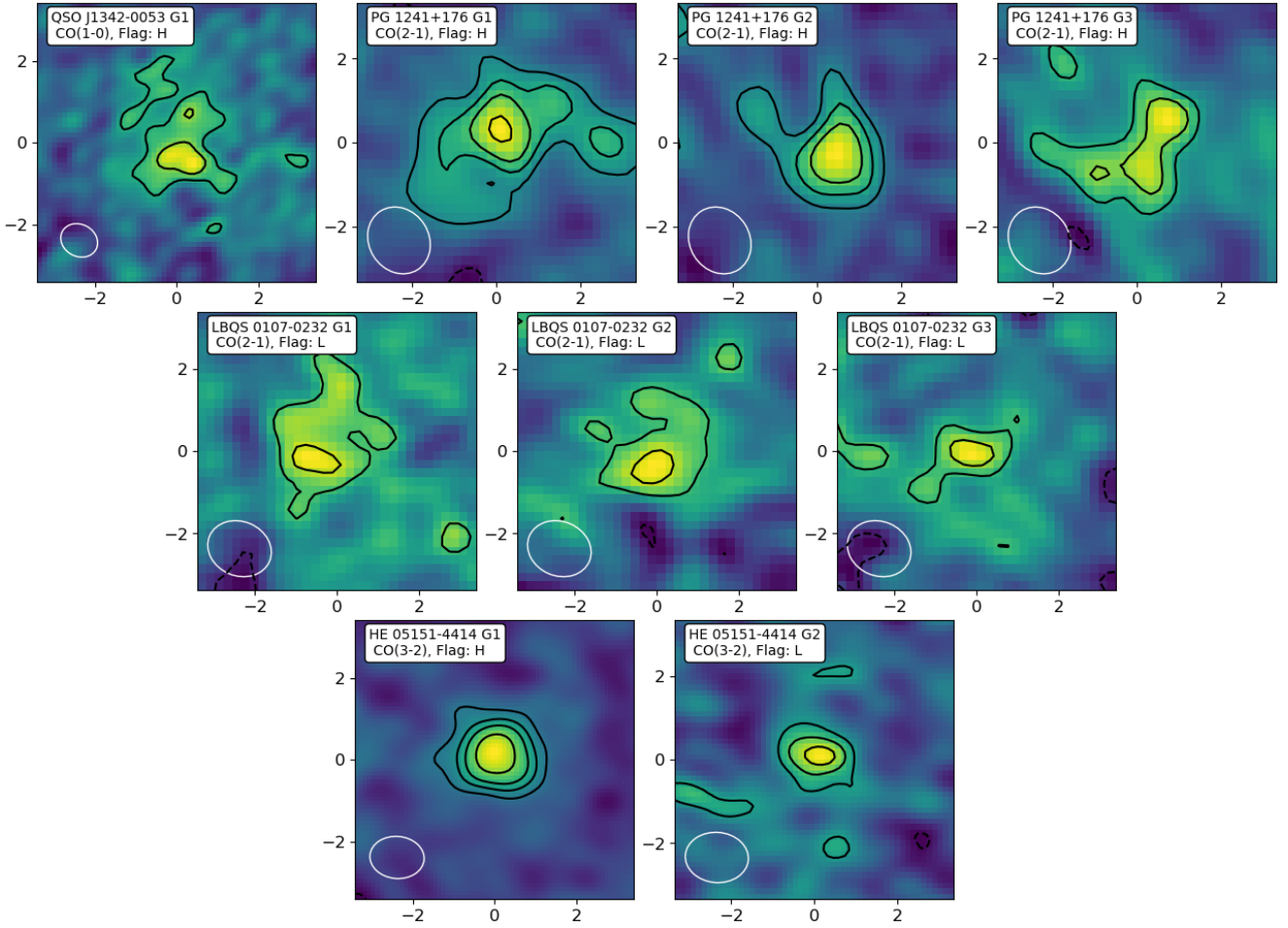


Figure 1. CO emission line maps for all absorption-selected galaxies in this sample. The maps show a $6 \times 6''$ wide field. Contours mark the 3, 5, 7, 10 sigma level in the integrated intensity plot, negative contours are plotted as dashed lines, the white ellipse shows the ALMA synthesized beam, the spectrum is extracted from the region where the integrated flux map is above 3 sigma. We also report the emission line and the confidence flag in the plot labels. The confidence flags (H: high, L: low) are discussed in Section 3. We report nine CO detections of host galaxies in close proximity to four absorbers with three absorbers showing significant galaxy overdensities.

et al. (2017). We carefully examine the positions of the galaxies presented by the authors of this work, however, we also do not detect any low confidence emission from these galaxies. Szakacs et al. (2021) have followed-up this field in CO(3-2) to a higher SNR. They report CO emission from one associated galaxy (SFR = $2.0 M_{\odot} \text{ yr}^{-1}$, $L = 0.6 L_{\star}$). We calculate an upper limit of the CO(2-1) emission

at the position of this galaxy which is consistent with the detection by Szakacs et al. (2021) (assuming a Milky Way type CO line ratio $L'_{\text{CO}(3-2)}/L'_{\text{CO}(2-1)} = r_{32} = 0.54$; Bolatto et al. 2013). We include this field in the further analysis using the CO(3-2) detection.

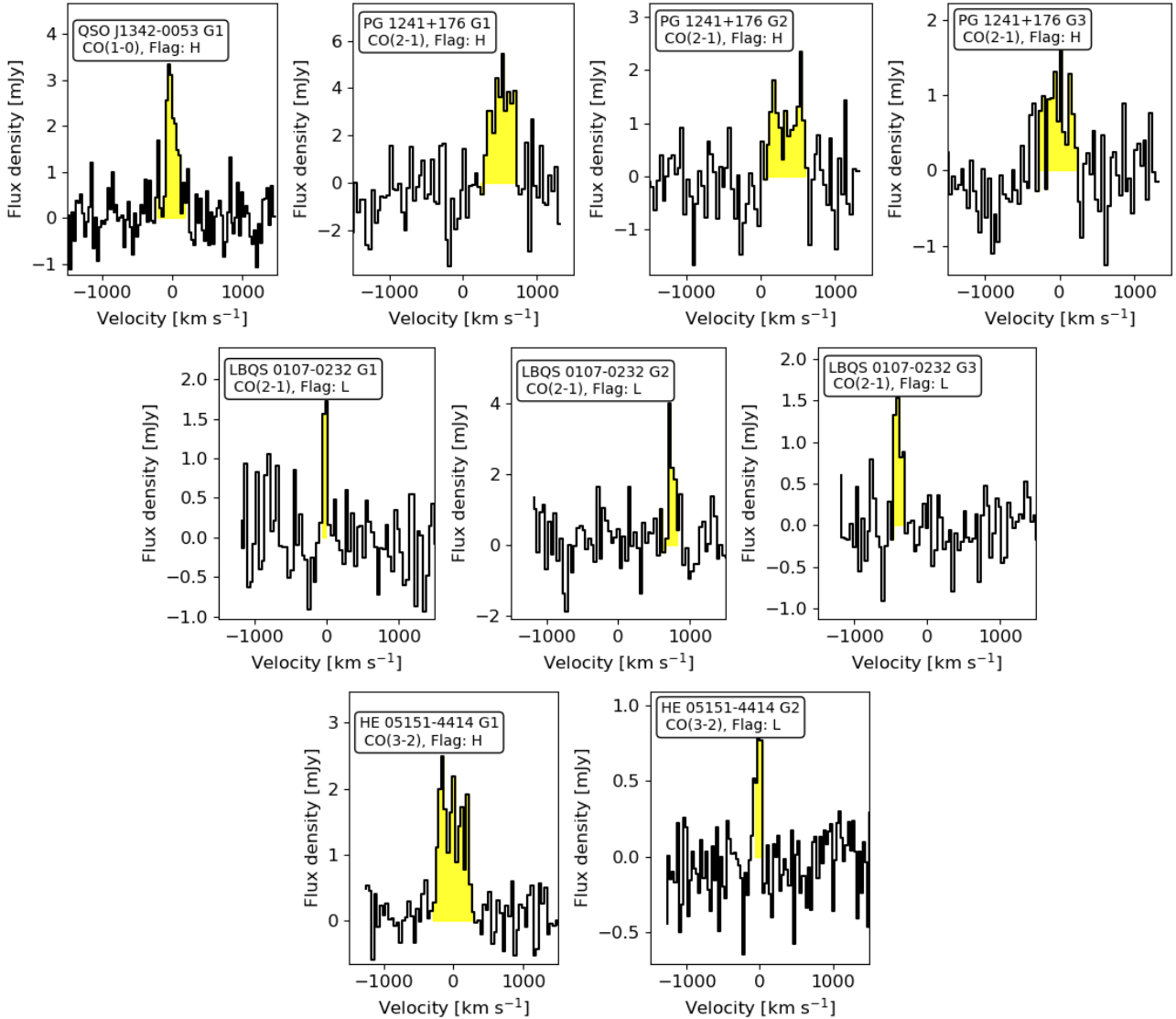


Figure 2. CO emission line spectra for all absorption-selected galaxies in this sample. The spectra are extracted from the region where the integrated intensity maps in Fig. 1 are above 3 sigma, spectra are PB corrected and re-binned for display. The zero velocity is set to the systemic velocity of the galaxy with the smallest impact parameter. We also report the emission line and the confidence flag in the plot labels. The confidence flags (H: high, L: low) are discussed in Section 3.

Table 2. Details of the ALMA observations.

Field	CO line	ALMA Band	RMS [mJy/beam]	beam [″ × ″]	beam [kpc × kpc]
QSO J0120-28	1-0	3	0.62	1.0 × 0.8	3 × 3
Q1342-0053	1-0	3	0.33	0.9 × 0.8	3 × 3
PKS 2128-123	2-1	4	0.90	0.9 × 0.8	5 × 5
PG 1241+176	2-1	4	0.50	1.6 × 1.4	11 × 9
Q0107-0232	2-1	4	0.42	1.6 × 1.3	10 × 9
HE 05151-4414	3-2	4	0.34	1.5 × 1.2	12 × 10

Q1241+176 ($z_{\text{abs}} = 0.55048$) In this field, we detect three galaxies at the absorber redshift. The galaxies lie at impact parameters of 60 – 120 kpc. In addition, [Steidel et al. \(1994\)](#) have identified a host galaxy at an impact parameter of 21.2 ± 0.3 kpc. However, the exact

details of this detection are not reported. We carefully search for CO emission at this impact parameter, but do not report a host galaxy.

Q0107-0232 ($z_{\text{abs}} = 0.55733$) [Crighton et al. \(2013\)](#) have identified two galaxies within $< 2''$ of the quasar sight-line in K-band imaging. If these galaxies were at the absorber redshift this would translate to impact parameters of 10 kpc and 11 kpc. We do not find CO emission from the position of these galaxies. However, we note that there is no redshift information available for these galaxies and these could be a chance alignment. We therefore exclude these galaxies as the absorber hosts. Instead, we detect three galaxies at impact parameters of 60 – 140 kpc. Given the narrow FWHM of these CO emission lines we label those as low confidence detections. In the further analysis these galaxies are excluded when drawing general conclusions.

Table 3. Molecular gas physical properties of galaxies associated with the absorbers.

Name	Flag	RA	Dec	Θ [kpc]	v_0 [km s ⁻¹]	FWHM [km s ⁻¹]	S_{int} [Jy km s ⁻¹]	S_{peak} [Jy]	$L'_{\text{CO}} \times 10^9$ [K km s ⁻¹]	$M_{\text{mol}} \times 10^9$ [M _⊙]
QSO J0120–28	-	-	-	-	-	-	< 0.94	-	< 1.6	< 6.8
QSO J1342–0053 G1	H	13h42m51.85s	-00d53m54.2s	35	-9	165 ± 8	0.59 ± 0.06	4.0 ± 0.7	1.5 ± 0.1	6.5 ± 0.6
Q2131–1207 G1 2-1	-	-	-	52	-	-	< 1.57	-	< 3.8	< 8.2
Q2131–1207 G1 3-2 ^a	H	-	-	52	-	184 ± 50	0.355	-	-	5.29
PG 1241+176 G1	H	12h44m09.59s	+17d20m58.1s	120	620	500 ± 10	1.49 ± 0.19	7.0 ± 1.8	5.9 ± 0.8	12.8 ± 1.6
PG 1241+176 G2	H	12h44m10.00s	+17d20m58.1s	86	460	300 ± 10	0.64 ± 0.09	3.0 ± 0.8	2.5 ± 0.3	5.5 ± 0.7
PG 1241+176 G3	H	12h44m10.64s	+17d20m55.6s	60	100	360 ± 10	0.41 ± 0.06	2.2 ± 0.6	1.6 ± 0.2	3.5 ± 0.5
LBQS 0107–0232 G1	L	01h10m14.22s	-02d17m06.6s	63	-291	60 ± 10	0.13 ± 0.02	2.4 ± 0.6	0.5 ± 0.1	1.1 ± 0.2
LBQS 0107–0232 G2	L	01h10m15.56s	-02d17m12.4s	144	449	240 ± 10	0.39 ± 0.07	4.7 ± 1.0	1.6 ± 0.3	3.4 ± 0.6
LBQS 0107–0232 G3	L	01h10m14.82s	-02d17m06.6s	69	-651	140 ± 10	0.17 ± 0.03	1.7 ± 0.5	0.7 ± 0.1	1.5 ± 0.2
HE 05151–4414 G1	H	05h17m08.51s	-44d10m51.4s	82	-188	600 ± 10	0.80 ± 0.06	2.6 ± 0.5	6.2 ± 0.5	7.2 ± 0.5
HE 05151–4414 G2	L	05h17m07.12s	-44d11m01.5s	67	-213	105 ± 8	0.08 ± 0.01	0.8 ± 0.3	0.6 ± 0.1	0.7 ± 0.1

Notes: The flag column shows the confidence (H: high, L: low) we assign to the detection. For more information see Section 3. Θ denotes the impact parameter measured between the QSO sight line and the galaxy position. v_0 is the velocity difference between the H₂ velocity centroid and the CO emission of the galaxy. The uncertainties in the molecular gas mass only include the flux measurement uncertainty, uncertainties in the conversion factors are discussed in Section 3.2. Upper limits are calculated assuming a 5σ detection threshold and a linewidth of 300 km s⁻¹. For QSO J0120–28 we use the sensitivity in the center of the image cube since no reliable counterpart has been reported. For Q2131–1207 we give the upper limit at the position of the optical counterpart reported by Péroux et al. (2017) and Szakacs et al. (2021). ^a In addition, we list as Q2131–1207 G1 3-2 the CO(3-2) measurement reported by Szakacs et al. (2021).

HE 0515–414 ($z_{\text{abs}} = 1.15$) We have identified two galaxies at the absorber redshift (one high and one low confidence) with impact parameters of 67 and 85 kpc.

This field was also observed using WFC3/G141 HST GRISM spectroscopy (PI: Bielby, ID: 14594). They have detected 9 galaxies at $z = 1.14 - 1.16$ within a field-of-view of 6' out of which one is G1 that we detect in CO (Bielby private comm.). Other galaxies identified in these data are outside the field-of-view of our ALMA observations.

We have obtained additional archival MUSE observations described in Section 2.3. We search for counterparts of the CO detected galaxies. At the absorber redshift the [OII] line is covered by the MUSE spectral range. We detect [OII] emission from G1, but not from G2. The [OII] emission line profile and emission line map are shown in Fig. A1. Following the description by Kennicutt (1998) we measure a non dust-corrected SFR of 9.4 M_⊙ yr⁻¹ which represents a lower limit on the true SFR. This translates to an upper limit for the molecular gas depletion time of 0.8 Gyr. This is in contrast to the long gas depletion times for absorption selected galaxies at intermediate redshifts reported by Kanekar et al. (2018); Péroux et al. (2019) and Szakacs et al. (2021).

Additionally, we use the [OII] and CO observations of G1 to study the ionised and molecular gas kinematics. The line of sight velocity maps are shown in Fig. A2. The CO line emission is only marginally resolved and the [OII] emission is not significant enough to allow for a detailed analysis using state-of-the-art forward modelling techniques. However, a qualitative analysis shows that the molecular and ionized gas kinematics are coupled. Both show rotation with similar orientation and maximum velocity.

3.2 Molecular gas masses

We convert the CO emission line luminosities in the observed transitions to the CO(1-0) line luminosity using a Milky Way type line ratio as reported by Carilli & Walter (2013). As we have no further information on the CO line excitation this assumption yields an upper limit of the molecular gas mass. We stress that previous studies of the CO spectral line energy distribution of absorption-selected

galaxies have in some cases shown more excited ISM conditions than that of the Galaxy (Klitsch et al. 2019). The CO(1–0) line fluxes could therefore be overestimated by a factor of 2 – 4. We have used a CO-to-H₂ conversion factor of $\alpha_{\text{CO}} = 4.36 M_{\odot} (\text{K km s}^{-1} \text{pc}^2)^{-1}$ that is applicable for galaxies of solar metallicity that do not undergo a starburst (including a factor of 1.36 to account for the presence of helium Bolatto et al. 2013). We caution, however, that the true molecular gas mass might be overestimated by up to a factor of six compared to $\alpha_{\text{CO}} = 0.8 M_{\odot} (\text{K km s}^{-1} \text{pc}^2)^{-1}$, appropriate for starburst environments. In case of a systematically too high conversion factor chosen for all galaxies the relative trends remain the same. If, however, only some galaxies in this sample have a Milky Way type CO line ratio and α_{CO} while for others a starburst type conversion is more appropriate this could introduce also relative shifts.

4 DISCUSSION

4.1 Detection rate

In this study we have selected the targets based on previously identified H₂-bearing gas detected in absorption instead of a metallicity based selection that has sometimes been used in previous such surveys. We find that the absorbers cover a range of 1/10th to solar metallicity. We list the molecular gas column density as well as the metallicity of the absorbers in Table 1. We find molecular gas-rich galaxies in five out of six fields and we detect multiple galaxies in three absorber fields. It is known from archival MUSE observations that in a fourth field (Q2131–1207) an overdensity of four galaxies is detected (Péroux et al. 2017). This success rate of > 80 per cent is remarkable for a study of molecular gas in absorption-selected systems. Similar studies at intermediate and high redshift focussing on high metallicity absorbers achieved a detection rate of ~ 40 – 70 per cent with a clear relation to the absorber metallicity (Kanekar et al. 2018; Kanekar et al. 2020; Szakacs et al. 2021). We attribute the higher detection rate of CO emission to the presence of the H₂-bearing clouds in absorption that indicate the presence of particularly molecular gas-rich systems.

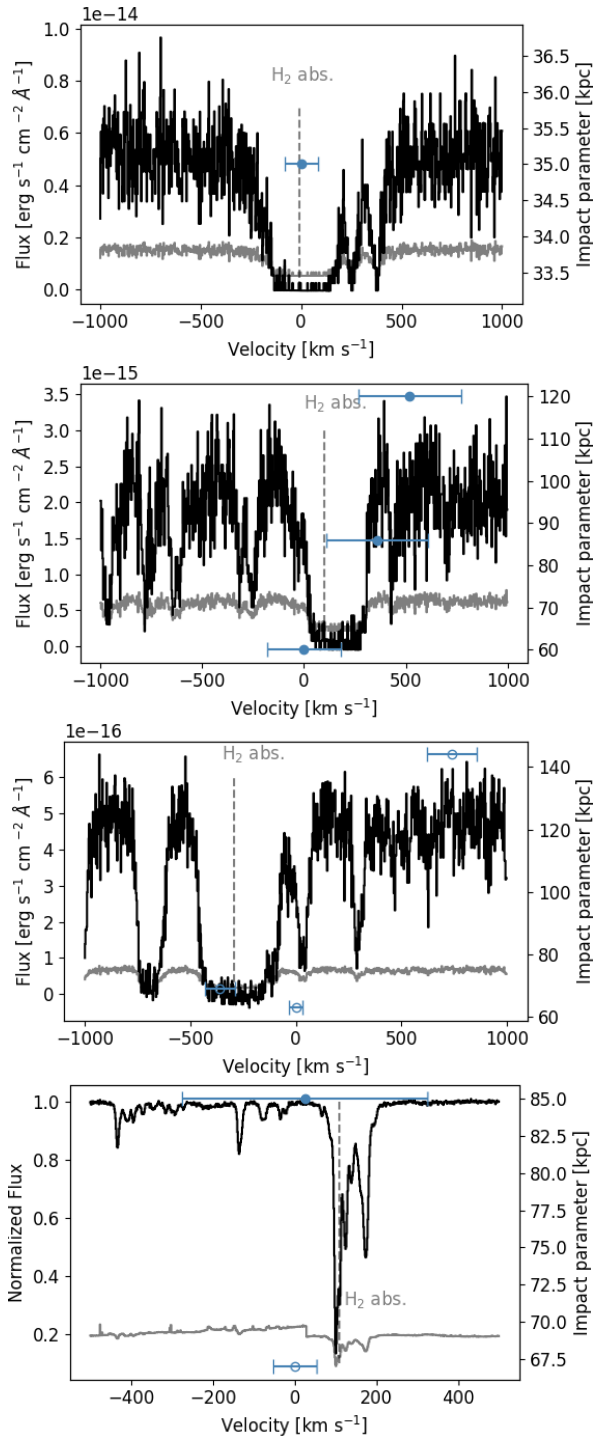


Figure 3. Comparison between absorption profiles and the galaxy detections in CO. The absorption lines shown are QSO1342: Ly α (HST COS), PG1241: Ly δ (HST COS), LBQS0107: Ly δ (HST COS), HE 0515: MgI 2852Å(UVES). The zero velocity refers to the systemic velocity of the host galaxy with the smallest impact parameter. Blue points mark the velocity offset of the CO detections, the errorbar width marks the FWHM, the vertical position marks the impact parameter from the quasar (see right axis). Filled and open symbols represent the high and low significance flags described in Section 3. The grey vertical dashed line marks the centroid of the H₂ absorption. Different absorption components around the main Ly transition are interlopers from the dense Ly α forest. The MgI absorption for HE0515 shows several velocity components spreading from $-100 - 250 \text{ km s}^{-1}$ that all belong to the same absorber.

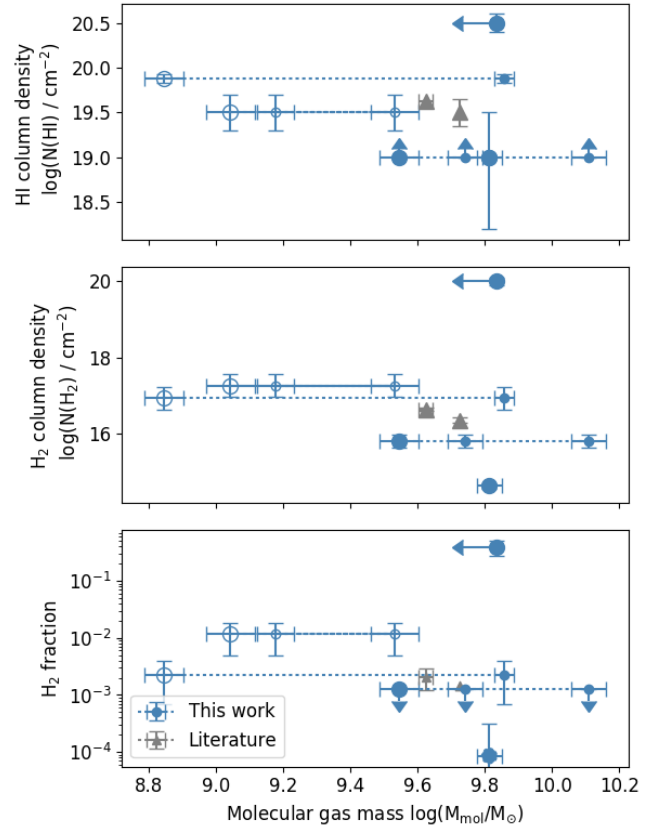


Figure 4. HI and H₂ absorber column density and molecular gas fraction as a function of molecular gas mass of the host galaxies (top to bottom). Larger markers indicate the galaxy with the smallest impact parameter. Filled and open symbols represent the high and low significance flags described in Section 3. Grey markers represent literature measurements from (Neelaman et al. 2016; Szakacs et al. 2021). We report no clear trend of absorption properties with the molecular gas mass of the host galaxies in both the full and the high significance sample. This suggests that H₂ absorption is tracing pockets of H₂-bearing gas in the outskirts of the CGM rather than an extended molecular disk.

4.2 Absorption associated to galaxy overdensities rather than single galaxies

A remarkable finding of this work is the detection of multiple galaxies associated to one absorber in most fields (three out of four fields presented here and in Q2131-1207 presented by Péroux et al. 2017; Szakacs et al. 2021). For the field of HE0515-4414 we report an even more extended structure of galaxies including 10 galaxies within $\sim 3 \text{ Mpc}$. A similar finding was reported by Hamanowicz et al. (2020) who present a sample of absorption-selected galaxies with follow-up VLT/MUSE IFU observations.

We test if the observed multiple galaxies are indeed overdensities by calculating the expected number of galaxies within the co-moving volume traced by our observations. We use the CO luminosity function reported by Fletcher et al. (2021) and integrate with a lower limit of 10^9 K km s^{-1} which is equivalent to the faintest detections in our sample. We find that at both, the low and high redshift end of our targets we expect fewer than one galaxy within the volume probed by the ALMA Band 3 and 4 observations. Here we consider a velocity range of $\pm 1000 \text{ km s}^{-1}$ from the absorber redshift. This suggests that

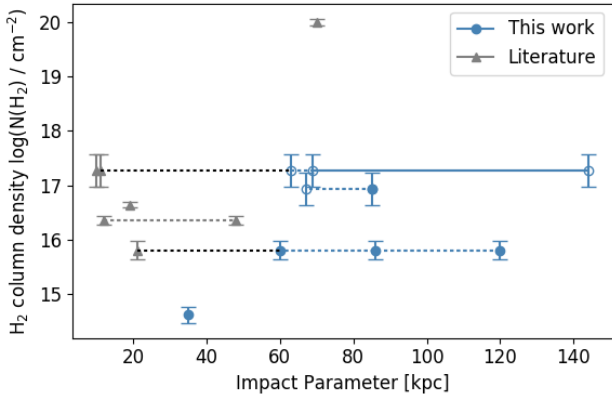


Figure 5. H_2 column density as a function of impact parameter for the detected galaxies in this work (blue, filled - high significance, open - low significance) and galaxies presented in the literature (Neeleman et al. 2016; Oliveira et al. 2014; Crighton et al. 2013; Szakacs et al. 2021). The lack of a correlation between H_2 molecular gas column density and the impact parameter in both samples (full and high significance) suggests that the absorption is not tracing extended molecular gas distributions.

the multiple galaxies detected in each field represent overdensities in the galaxy distribution at the absorber redshift.

4.3 Molecular gas mass relation to absorber properties

Although the sample size is limited and the connection between absorber and host galaxies might be complex due to identification of multiple host galaxies, we test if we can find a relation between the molecular gas mass of the absorption-selected galaxies and the absorber properties. In Fig. 4 we show the $H\text{I}$ column density, the H_2 column density and the molecular gas fraction as a function of the molecular gas mass of the host galaxies. We do not report a significant correlation in any of these parameter spaces for both, the full sample and the high significance detections only. This is probably expected as the connection between the absorber and the host galaxy in such complex systems is not straightforward. A similar non-correlation was identified in optical studies finding galaxy overdensities related to absorbers in a similar redshift range (Hamanowicz et al. 2020).

4.4 Do molecular gas absorbers probe disks of galaxies or pockets of dense gas in the CGM?

To test whether the H_2 -bearing gas traces disks of galaxies or pockets of dense gas in the circum-galactic medium (CGM) we analyse the distance between the absorber and the host galaxies in both projected distance on sky (impact parameter) and distance in velocity space to probe the full extent of the three dimensional structure. In Fig. 3 we show the absorption profiles in relation with emission line width of the CO detected galaxies in terms of both sky position (right y-axis) and velocity space (x-axis). The lack of comparison spectra of strong metal absorption lines often hampers a direct comparison. For some sight lines the only available lines are embedded in the $\text{Ly}\alpha$ forest making a comparison between the absorption components and CO emission lines challenging.

We find large impact parameters of 35 – 140 kpc suggesting that the molecular absorption does not probe the extended molecular disk of a single galaxy. In addition, we find a good agreement between

the absorption and CO emission in velocity space. This suggests an association between the neutral and H_2 -bearing gas at the position of the quasar sight line and the molecular gas in the host galaxies.

Additionally, we test for a relation between the H_2 column density and the impact parameter (see Fig. 5), that would be expected if the absorption is tracing the disk of the host galaxy. We do not identify a clear trend between these two quantities adding further evidence that the absorption is tracing pockets of H_2 -bearing gas rather than the disk of a molecular gas-rich galaxy. Comparing the detection rates of our work with previous studies focussing on high metallicity we find that first with a success rate of > 80 per cent our detection rate is significantly higher and second we find overdensities of galaxies rather than single galaxies. This suggests that there is possibly more diffuse gas around overdensities of galaxies which provides the appropriate conditions for molecular gas to form in-situ or survive the outflow from a galaxy traced in absorption.

Galaxy interactions are numerous in overdense environments. Interactions can produce tidal streams as well as promote starburst or AGN driven outflows. The H_2 molecular gas could therefore be part of self-shielded, tidally stripped or ejected disk material. This scenario is supported by the observations of molecular gas in high velocity clouds in the Milky Way (Richter et al. 2001; Putman et al. 2012). Furthermore, the molecular gas could be transported out to large distances by outflows (Richings & Faucher-Giguere 2018).

We note that we cannot exclude the presence of low molecular gas mass galaxies below our detection limit at small impact parameters. Ideal follow-up observations to settle this question would be optical IFU observations to detect all galaxies in these fields down to low star formation rates.

5 CONCLUSIONS

In this paper we present a systematic search for molecular gas traced by CO emission in H_2 absorption selected systems. We report the detection of CO emission from galaxies in close proximity to absorbers in five out of six quasar fields (including the deeper observations presented by Szakacs et al. 2021). Our main conclusions can be summarised as follows:

- Our detection rate of > 80 per cent is higher than that reported in previous studies (Kanekar et al. 2018; Kanekar et al. 2020) suggesting that the H_2 -bearing gas absorbers trace CO molecular gas-rich galaxies.
- Interestingly, the only system without a CO detection has the lowest metallicity. However, the CO detected galaxies are related to absorbers with a wide range of absorption metallicities.
- The H_2 -bearing gas in absorption in all except two sight-lines traces galaxy overdensities. In the case of HE0515-4414 this is also supported by GRISM spectroscopy tracing scales of 3 Mpc. In the case of Q2131-1207 only one galaxy is detected in CO, but additional MUSE observations reveal three additional [OIII] emitting galaxies connected to the absorber. This adds further evidence that absorption selection is efficient at tracing overdense environments.
- In the case of HE0515-4414 G1, we gather first insights in the molecular and ionised gas kinematics traced by ALMA and MUSE observations, respectively. We find that both velocity fields qualitatively agree in orientation and maximum velocity. Deeper high resolution observations are necessary for a complete morpho-kinematic modelling.
- We detect galaxies at impact parameters of 35 – 144 kpc. We conclude that the H_2 -bearing absorbers do not trace the inner disk of a galaxy, but pockets of diffuse molecular gas in the circum-galactic

and intra-group medium. This is also supported by the lack of a clear correlation between the absorber column density or molecular gas fraction with impact parameter or host galaxy molecular gas mass.

ACKNOWLEDGEMENTS

The authors thank Palle Møller for important discussions related to this work and Roland Szakacs for sharing preliminary results. A.K. thanks Aleksandra Hamanowicz for important discussions related to this work. A.K. gratefully acknowledges support from the Independent Research Fund Denmark via grant number DFF 8021-00130. A.D.C. acknowledges support by the Swiss National Science Foundation under grant 185692. S.L. was funded by FONDECYT grant number 1191232. This paper makes use of the following ALMA data: ADS/JAO.ALMA#2018.1.01575.S. ALMA is a partnership of ESO (representing its member states), NSF (USA) and NINS (Japan), together with NRC (Canada), MOST and ASIAA (Taiwan), and KASI (Republic of Korea), in cooperation with the Republic of Chile. The Joint ALMA Observatory is operated by ESO, AUI/NRAO and NAOJ. In addition, publications from NA authors must include the standard NRAO acknowledgement: The National Radio Astronomy Observatory is a facility of the National Science Foundation operated under cooperative agreement by Associated Universities, Inc. This research made use of Astropy¹ a community-developed core Python package for Astronomy (Astropy Collaboration et al. 2013; Price-Whelan et al. 2018). This research has made use of NASA's Astrophysics Data System.

DATA AVAILABILITY

The data underlying this article are available in the respective observatories online archives. Used ALMA data is available through the ALMA Science Archive (<https://almascience.eso.org/asax/>), VLT/MUSE data is available through the ESO SciencenArchive Facility (<http://archive.eso.org/cms.html>) and HST data through the Hubble Legacy Archive (<https://hla.stsci.edu>). Project IDs are given in Section 2 and 3.

REFERENCES

- Astropy Collaboration et al., 2013, *A&A*, 558, A33
 Bielby R., Crighton N. H. M., Fumagalli M., Morris S. L., Stott J. P., Tejos N., Cantalupo S., 2017, *MNRAS*, 468, 1373
 Boettcher E., et al., 2020, arXiv:2010.11958 [astro-ph]
 Bolatto A. D., Wolfire M., Leroy A. K., 2013, *ARA&A*, 51, 207
 Bolmer J., et al., 2019, *A&A*, 623, A43
 Carilli C., Walter F., 2013, *ARA&A*, 51, 105
 Crighton N. H. M., et al., 2013, *MNRAS*, 433, 178
 Fletcher T. J., Saintonge A., Soares P. S., Pontzen A., 2021, *MNRAS*, 501, 411
 Fynbo J. P. U., et al., 2018, *MNRAS*, 479, 2126
 Hamanowicz A., et al., 2020, *MNRAS*, 492, 2347
 Kanekar N., et al., 2018, *ApJL*, 856, L23
 Kanekar N., Prochaska J. X., Neeleman M., Christensen L., Møller P., Zwaan M. A., Fynbo J. P. U., Dessauges-Zavadsky M., 2020, *ApJ*, 901, L5
 Kennicutt Jr. R. C., 1998, *ApJ*, 498, 541
 Klitsch A., Péroux C., Zwaan M. A., Smail I., Oteo I., Biggs A. D., Popping G., Swinbank A. M., 2018, *MNRAS*, 475, 492
 Klitsch A., et al., 2019, *MNRAS*, 482, L65

- Lofthouse E. K., et al., 2020, *MNRAS*, 491, 2057
 McMullin J. P., Waters B., Schiebel D., Young W., Golap K., 2007, *Astronomical Data Analysis Software and Systems XVI*, 376, 127
 Møller P., et al., 2018, *MNRAS*, 474, 4039
 Muzahid S., Srianand R., Charlton J., 2015, *MNRAS*, 448, 2840
 Muzahid S., Kacprzak G. G., Charlton J. C., Churchill C. W., 2016, *ApJ*, 823, 66
 Neeleman M., et al., 2016, *ApJL*, 820, L39
 Neeleman M., Kanekar N., Prochaska J. X., Christensen L., Dessauges-Zavadsky M., Fynbo J. P. U., Møller P., Zwaan M. A., 2018, *ApJ*, 856, L12
 Oliveira C. M., Sembach K. R., Tumlinson J., O'Meara J., Thom C., 2014, *ApJ*, 783, 22
 Péroux C., Howk J. C., 2020, *ARA&A*, 58, 363
 Péroux C., et al., 2017, *MNRAS*, 464, 2053
 Péroux C., et al., 2019, *MNRAS*, 485, 1595
 Price-Whelan A. M., et al., 2018, *AJ*, 156, 123
 Putman M. E., Peek J. E. G., Jounge M. R., 2012, *ARA&A*, 50, 491
 Quast R., Reimers D., Baade R., 2008, *A&A*, 477, 443
 Rao S. M., Turnshek D. A., Nestor D. B., 2006, *ApJ*, 636, 610
 Reimers D., Baade R., Quast R., Levshakov S. A., 2003, *A&A*, 410, 785
 Rhodin N. H. P., Christensen L., Møller P., Zafar T., Fynbo J. P. U., 2018, *A&A*, 618, A129
 Richings A. J., Faucher-Giguere C.-A., 2018, *MNRAS*, 474, 3673
 Richter P., Sembach K. R., Wakker B. P., Savage B. D., 2001, *ApJ*, 562, L181
 Schroetter I., et al., 2021, *MNRAS*,
 Som D., Kulkarni V. P., Meiring J., York D. G., Péroux C., Lauroesch J. T., Aller M. C., Khare P., 2015, *ApJ*, 806, 25
 Steidel C. C., Dickinson M., Persson S. E., 1994, *ApJ*, 437, L75
 Szakacs R., et al., 2021, arXiv e-prints, p. arXiv:2105.07280
 Werk J. K., Prochaska J. X., Thom C., Tumlinson J., Tripp T. M., O'Meara J. M., Peeples M. S., 2013, *ApJS*, 204, 17
 Werk J. K., et al., 2014, *ApJ*, 792, 8
 Wolfe A. M., Gawiser E., Prochaska J. X., 2005, *ARA&A*, 43, 861

APPENDIX A: LINE OF SIGHT VELOCITY MAPS OF THE IONISED AND MOLECULAR GAS IN HE0515-4414 G1

This paper has been typeset from a $\text{\TeX}/\text{\LaTeX}$ file prepared by the author.

¹ <http://www.astropy.org>

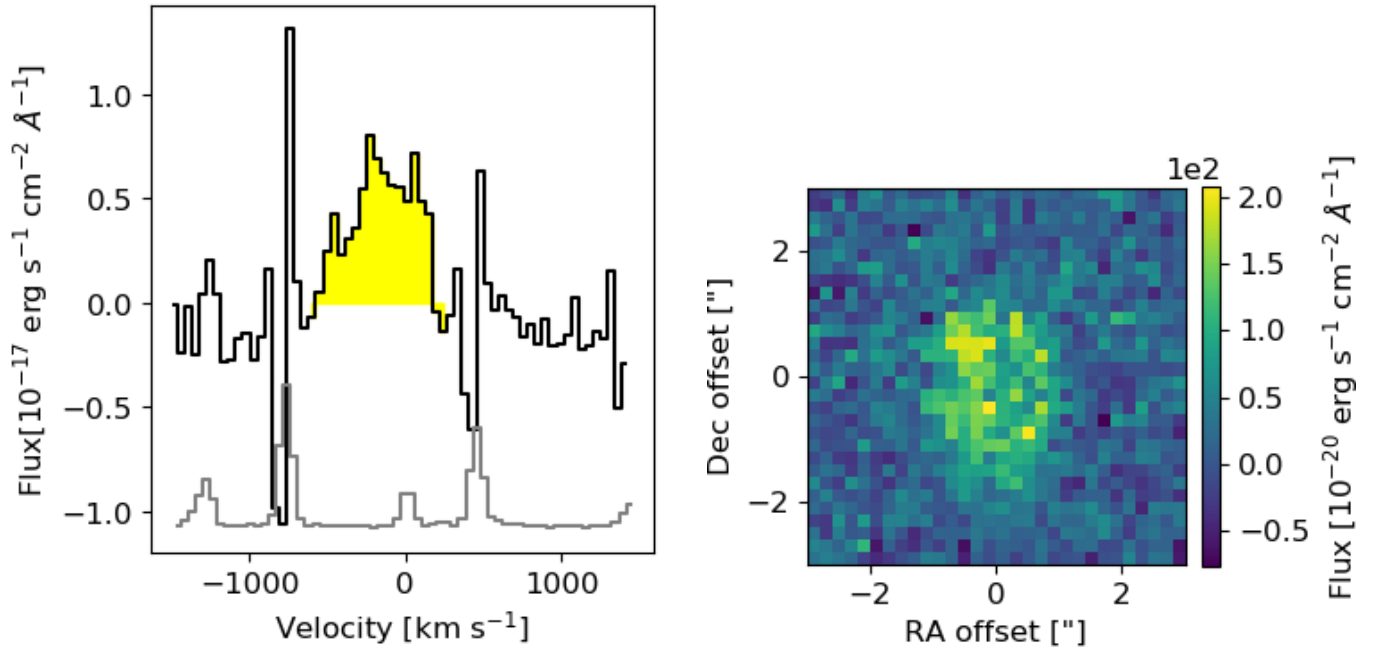


Figure A1. Ionized gas observations of HE 0515-4414 Galaxy 1 ($z = 1.15$) traced by [OII] emission observed using MUSE. *Left:* spectrum of the [OII] emission line, where the zero velocity marks the position of the absorber. *Right:* integrated intensity map of the [OII] emission line integrated over the yellow region marked in the spectrum.

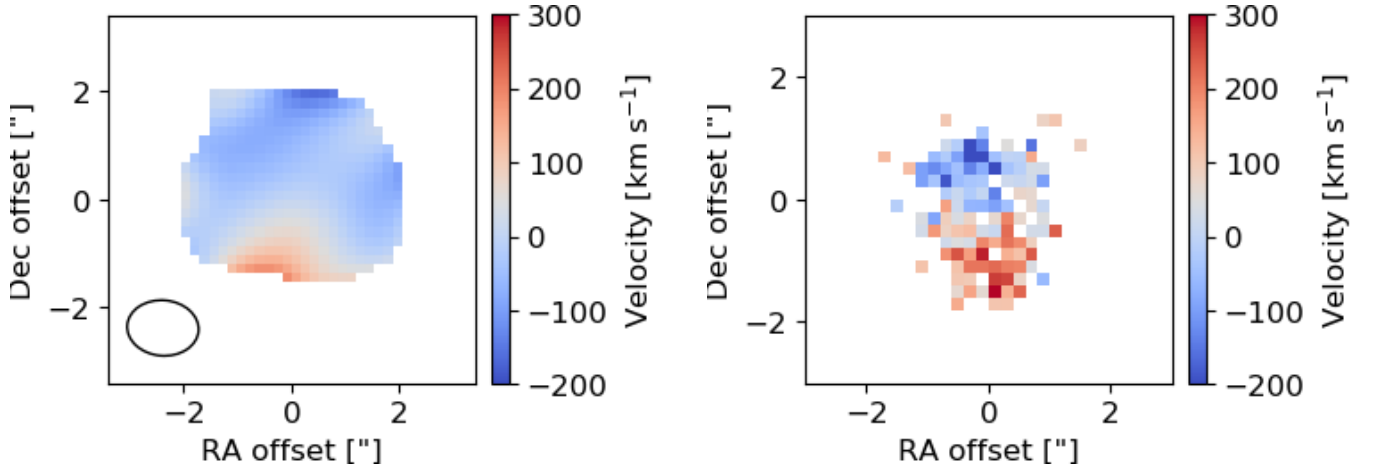


Figure A2. Line of sight velocity map of the molecular gas traced by CO(3-2) observed using ALMA (*left*) and the ionized gas traced by [OII] observed using MUSE (*right*) in HE 0515-4414 Galaxy 1.